Polyion complex hydrogels from chemically modified cellulose nanofibrils: Structure-function relationship and potential for controlled and pH-responsive release of doxorubicin

Sry D. Hujaya,[a] Gabriela S. Lorite,[b] Seppo J. Vainio,[c] Henrikki Liimatainen*,[a]

[a] Fibre and Particle Engineering Research Unit, University of Oulu, P. O. Box 4300, FI-90014 Oulu, Finland

[b] Microelectronics Research Unit, University of Oulu, P. O. Box 4500, FI-90014, Finland

[c] Laboratory of Developmental Biology, Biocenter Oulu, University of Oulu, P. O. Box 5000, FI-90014 Oulu, Finland

KEYWORDS: nanocellulose; cellulose nanofibrils; hydrogel; polyion complex; controlled release; pH-responsive; doxorubicin; cancer

Abstract

Herein, we report the fabrication of a polyion complex hydrogel from two oppositely charged derivatives of cellulose nanofibrils (CNF). CNF was produced from dissolving pulp through subsequent periodate oxidation, chemical modification, and microfluidization. Three different durations for periodate oxidation (30 min, 120 min, and 180 min) resulted in three different aldehyde contents. Further, two types of chemical modifications were introduced to react with the resulting aldehydes: chlorite oxidation to yield anionic CNF with carboxylic acid groups (DCC) and imination with Girard's reagent T to yield cationic CNF containing quaternary ammonium groups (CDAC). Functional group contents were assessed using conductometric titration and elemental analysis, while nanofibril morphologies were assessed using atomic force microscopy (AFM). Longer durations of periodate oxidation did not yield different width profile but was found to decrease fibril length. The formation of self-standing hydrogel through mixing of DCC and CDAC dispersions was investigated. Oscillatory rheology was performed to assess the relative strengths of different gels. Self-standing hydrogels were obtained from mixture of DCC180 and CDAC180 dispersions in acetate buffer at pH 4 and 5 at a low concentration of 0.5% w/w that displayed approximately 10-fold increase in storage and loss moduli compared to those of the individual dispersions. Self-standing gels containing doxorubicin (an anticancer drug) displayed pH-responsive release profiles. At physiological pH 7.4, approximately 65% of doxorubicin was retained past a burst release regime, while complete release was observed within 5 days at pH 4. Biocompatibility of DCC180, CDAC180, and their mixture were investigated through quantification of the metabolic activity of NIH3T3 cells *in vitro*. No significant cytotoxicity was observed at concentrations up to 900 µg/mL. In short, the nanocellulose-based polyion complex hydrogels obtained in this study are promising nature-derived materials for biomedical applications.

Graphical Abstract

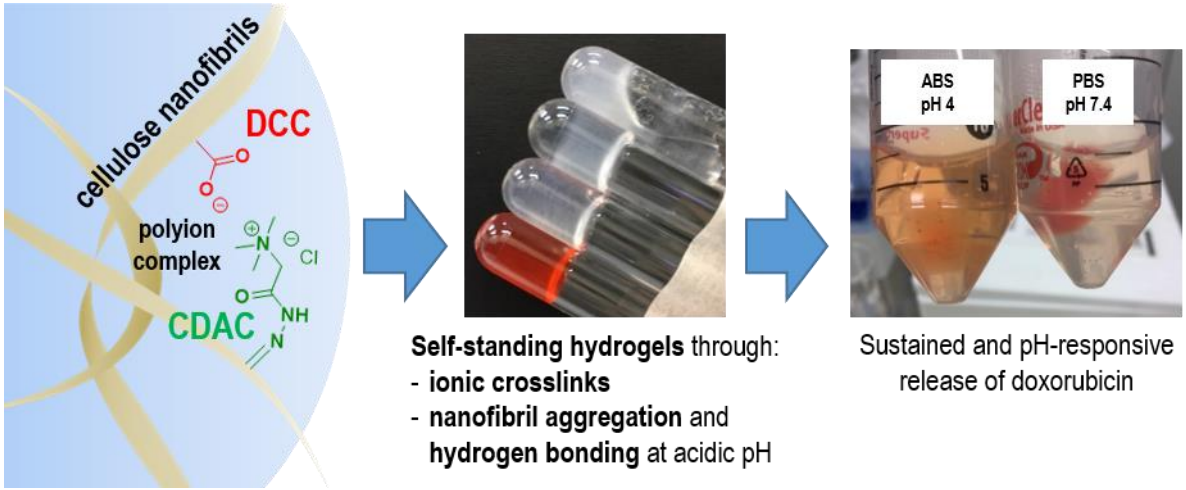

1. Introduction

Hydrogels are promising materials, especially for biomedical applications, due to their excellent water-retention capability and biocompatibility. Hydrogels from various synthetic and natural materials have been engineered and commercialized into drug delivery systems, wound dressings, contact lenses, hygiene products, and cell culture scaffolds for tissue engineering, as recently reviewed [1].

Nanocellulose is a natural material composed of highly structured cellulose chains that have at least one dimension in the nanoscale. Cellulose nanofibrils (CNFs), a class of elongated and flexible nanocelluloses, have a typical elementary nanofibril width of 3-5 nm up to 20-50 nm associated with nanofibril aggregates, and a length from 500 nm to a few microns [2]. CNFs are usually obtained through an intensive mechanical disintegration process (also referred to as fibrillation or microfluidization), which is preceded by chemical pretreatment to reduce energy consumption. The morphology of CNF is highly influenced by the specific chemical and physical treatments. Chemical pretreatment facilitates fibrillation by providing charged groups that cause repulsion and disintegration. Consequently, the final CNF is also a derivative of the original native cellulose, which can contain functional chemical moieties that can be beneficial for the application of the CNF final products.

Upon fibrillation, the highly entangled nanofibrillar network retains a large amount of water, thus making CNF an inherent hydrogel. In the biomedical field, studies have shown that CNF-based hydrogels and cellulose nanocomposites can be used as a matrix for controlled release of drugs [3, 4], as biomedical implants [5], and as a 3D-matrix for tissue engineering [6, 7]. However, most reports on the biomedical applications of CNF have utilized a monocomponent CNF system [3, 7-9] or a composite system of CNF with water-soluble polymers [10-12]. The inherent physical differences between CNF and macromolecular water-soluble polyelectrolytes warrant an investigation of the potential of utilizing polyion crosslinks as hydrogel network stabilizer. Herein, we report the fabrication of a novel type of polyion complex hydrogel from two oppositely charged derivatives of CNFs. To the best of our knowledge, this is the first report on the topic, and the results of this study may inspire a new approach to the utilization of CNF derivatives for biomedical applications.

In this report, two derivatives of CNF: DCC which contains negatively-charged carboxylic acid group and CDAC which contains positively-charged quaternary ammonium group were prepared as shown in Scheme 1, and physically mixed to facilitate gelation. The propensity for forming self-standing hydrogels was studied through rheological characterizations of the CNF dispersions before and after mixing in various pH values and ionic strength conditions. The structure-function relationship was studied by connecting the

morphologies of the nanofibrils and the functional group contents with relative gel strengths. Further, we demonstrate the applicability of the polyion complex hydrogels to provide controlled and pH-responsive release of doxorubicin hydrochloride (DOX), which is a primary amine-containing chemotherapeutic agent. Additionally, the biocompatibility of selected CNFs was investigated through an *in vitro* cell culture study. The results of this study further suggest that CNFs are promising green biomaterials for biomedical applications.

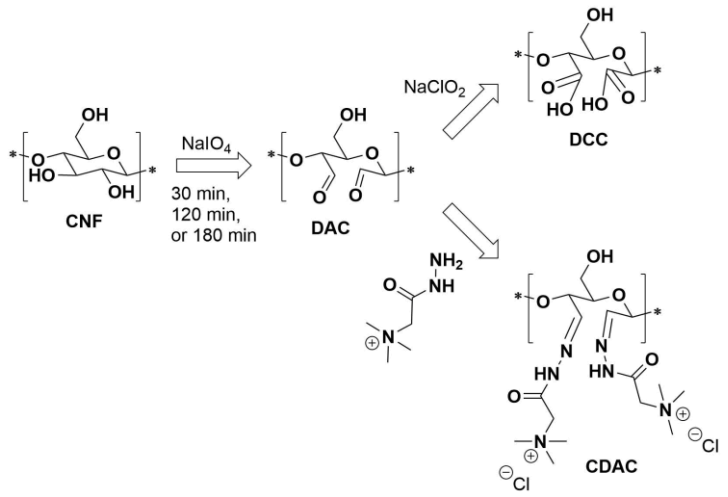

Scheme 1. Summary of synthetic pathways and chemical structures of DCC and CDAC cellulose nanofibrils.

2. Materials and Methods

Sodium periodate ($NaIO_4$, Sigma-Aldrich, Germany), sodium chlorite ($NaClO_2$, Sigma-Aldrich, Germany), acetic acid (CH_3COOH, Merck, Germany), Girard's reagent T (Acros Organics, USA), sodium chloride (NaCl, Merck, Germany), potassium chloride (KCl, Merck, Germany), sodium dihydrogen phosphate monohydrate ($NaH_2PO_4.H_2O$, Merck, Germany), disodium hydrogen phosphate dihydrate ($Na_2HPO_4.2H_2O$, Merck, Germany), acetic acid glacial, sodium acetate trihydrate (VWR Chemicals, Finland), and doxorubicin hydrochloride (DOX, TCI Chemicals, Japan) were purchased and used without further purification. Dissolving pulp was obtained from Domsjö Fabriker AB, Sweden (cellulose 96.2 %, hemicelluloses 3.5 %, total lignin <0.5 %, acetone soluble extractives 0.17%).

PBS buffer was prepared by dissolving NaCl, KCl, $NaH_2PO_4.H_2O$ and $Na_2HPO_4.2H_2O$ in the appropriate amounts in deionized water and by adjusting the pH using HCl or NaOH.

Acetate buffers (Ac) pH 4 and pH 5 were prepared by mixing 0.1 M acetic acid glacial and 0.1 M sodium acetate in the appropriate amounts in deionized water and by adjusting the pH using HCl or NaOH.

2.1. Syntheses of DCC and CDAC

Syntheses of DCC and CDAC followed the series of reactions depicted in Scheme 1. The resulting CNFs are designated DCC**X** or CDAC**X**, where **X** is the duration of the initial periodate oxidation of the dialdehyde cellulose (DAC, Scheme 1).

Syntheses of both DCC and CDAC were carried out by first immersing dissolving pulp in deionized water for at least 2 h, followed by mechanical disintegration. A 1 L dispersion containing 10 g of pulp was then brought to 55 °C in a water bath and reacted with sodium periodate (8.2 g) for a designated duration (30 min, 120 min, or 180 min) in the dark. The dispersion was then filtered through 12-15 µm filter paper and washed with at least 4 L of deionized water. DAC was used immediately due to the unstable nature of the aldehydes.

DCC was synthesized by reacting the respective DAC (4 g dry weight) with sodium chlorite in a 1 M acetic acid solution in deionized water for 2 days at room temperature. After the reaction, the product was filtered through 12-15 µm filter paper, washed with deionized water, and sampled for measurement of the dry matter content. The remaining product was suspended into a 1% w/w concentration in deionized water, the pH was adjusted to ~7 and then stirred at room temperature. Microfluidization was performed on a Microfluidics M-110EH-30 microfluidizer (USA). Dispersions were passed twice through a 200-µm chamber at a pressure of 1000 bar. The reaction recovery were 84% (DCC30), 88% (DCC120), and 104% (DCC180).

CDAC was synthesized by adding 4 g (dry weight) of DAC30, DAC120, or DAC180 into 400 mL of deionized water containing 4.09 g, 8.0 g, or 11.7 g of Girard's reagent T for CDAC30, CDAC120, and CDAC180, respectively, at pH 4.5. After stirring at room temperature for 3 days, the product was filtered through 12-15 µm filter paper, washed with deionized water, and sampled for measurement of the dry matter content. The remaining product was suspended into a 1% w/w concentration in deionized water and stirred at room temperature. Prior to microfluidization, the dispersion was first pretreated with an Ultra Turrax at 10 000 rpm for 5 min. Dispersions were passed twice through the 100-µm chamber of the microfluidizer at a pressure of 1000 bar. The obtained cellulose nanofibrils were designated as follows: CDAC30, CDAC120, or CDAC180. The reaction recovery were 82% (CDAC30), 88% (CDAC120), and 100% (CDAC180).

Microfluidization was performed using different chambers for both DCC and CDAC. The reported combinations were the optimal conditions to obtain CNF dispersions that were stable without flocculation as they were stored and used in the never-dried state.

2.2. Conductometric Titration

Carboxylic acid contents in DCC were determined in accordance with the conductometric titration protocol described by Rattaz *et al.* and Katz *et al.* using an Excellence Titrator T5 (Mettler Toledo, USA) [13, 14].

2.3. Elemental Analysis

Nitrogen content in CDAC samples was measured using an elemental analyzer (PerkinElmer 2400 Series II CHNS/O Analyzer, USA). Samples were dried *via* either oven drying or freeze drying and kept in a desiccator until measurements were performed.

2.4. Hydrogel Preparation

To prepare hydrogel samples, dispersions of DCC and CDAC were prepared by diluting the stock dispersions with the desired buffer solution to a concentration of 0.5% w/w. The following buffer solutions were used: 10 mM phosphate buffer pH 7.4 (PB), 10 mM phosphate buffer pH 7.4 containing 150 mM salt (PBS), 10 mM acetate buffer pH 5 (Ac5), and 10 mM acetate buffer pH 4 (Ac4). Then, 0.5 mL of CDAC dispersion was added to 0.5 mL of DCC in a small test tube under vortex, which was further maintained for at least another 5 seconds. Hydrogels were then left to equilibrate at 4-8 °C for at least 48 h.

DOX-loaded hydrogels were prepared by first dissolving DOX in an acetate buffer (pH 4), which was then used to dilute the DCC180 dispersion to a 0.5% w/w concentration. 0.5 mL of 0.5% w/w CDAC180 dispersion in deionized water was then added to the DOX-containing DCC180 dispersion under vortex. The final concentration of DOX in the hydrogels was 400 µg/mL.

To avoid ambiguity, throughout this report the bicomponent hydrogels will be referred to as gels or hydrogels, while the individual CNF dispersions will be referred to as dispersions. Gels are labeled (DCC**X**+CDACX)**Y**, where **X** is the periodate oxidation duration, and **Y** is the buffer type. For example, (DCC180+CDAC180)Ac4 indicates that the bicomponent hydrogel was prepared by mixing DCC180 and CDAC180 dispersions, with both dispersions having 0.5% w/w concentration in acetate buffer pH 4.

2.5. Dynamic Oscillatory Rheology

Rheological measurements were performed on a Discovery Hybrid Rheometer (DHR-01, TA Instruments) equipped with a cone-plate geometry with a diameter of 40 mm. The gap was set at 52 µm and water evaporation was prevented by applying droplets of water around the plate and covering with a custom-made cover. Oscillatory frequency sweep was carried out at 25 °C between 0.628 to 100 rad/s at a constant strain of 1%, which was previously confirmed to be within the linear viscoelastic region through a strain sweep (ω = 10 rad/s). For each type of gel, samples were prepared and measured in duplicate. Comparison of storage (G') and loss (G") moduli values was done by reporting the G' and G" values at the specific angular frequency of 9.96 rad/s.

2.6. Field Emission Scanning Electron Microscope (FESEM) Imaging

Hydrogel samples for FESEM imaging were prepared by immersing the as-prepared hydrogels into liquid nitrogen followed by freeze-drying (Scanvac Coolsafe 55–15 Pro, Denmark) for 2-3 days. Freeze-dried hydrogels were then mounted on top of a carbon-taped mount and sputter-coated with platinum. FESEM imaging was performed on a Zeiss Sigma FESEM (Germany). A low accelerating voltage of 5 kV was used during imaging.

2.7. Atomic Force Microscopy (AFM) Imaging and Statistical Measurement of Nanofibril Lengths and Widths

Atomic force microscopy images were acquired by using a MultiMode8 (Bruker, Germany) with ScanAsyst^{TM} in air and triangular Si probes (with a typical tip radius of 2 nm and a nominal spring constant of 0.4 N/m). Samples were prepared by first sonicating 0.001% w/w CNF dispersions in deionized water and drop casting ~20 µL on a freshly cleaved mica surface with a diameter of 12 mm (Ted Pella, USA). The water was then allowed to evaporate. Topography images were acquired at multiple 5 x 5 µm^2 scan areas to obtain individual nanofibrils for quantitative analyses of the width and length. For each sample, the width of about 200 nanofibrils was measured using Gwyddion software version 2.44. In addition, the length of about 350 nanofibrils was obtained using ImageJ software [15]. The plugin "Ridge Detection" was used to support the tracing of nanofibrils [16]. Highly entangled nanofibrils were excluded from length measurement but included in width measurement. Kinked nanofibrils were included, and the length was estimated as the longest sum of continuous segments connecting two ends. The width and length distributions were fitted to the lognormal function using OriginPro 2018 software (Origin Lab Corporation, USA). Additionally, number-average and length-weighted average length and width were also calculated from the collected data.

2.8. Doxorubicin Release Studies

DOX release profiles were studied by immersing 1 mL of DOX-loaded self-standing hydrogel containing 400 µg of DOX into 10 mL of release medium (either PBS buffer pH 7.4 or acetate buffer saline (ABS) pH 4 containing 150 mM of salt) at 37 °C. DOX-containing gels were immersed freely in the release medium and are able to maintain their shape throughout the experiment. At various intervals, 1 mL of the medium was collected and replaced with fresh medium. The collected media were measured using a UV spectrophotometer (UV-1800, Shimadzu, Japan) for the absorbance values at the λ_{max} of doxorubicin (480 nm). The amount of DOX in the release medium was calculated by correlating to a standard curve recorded from a dilution series of DOX solution of known concentration in the same buffer as the release medium. Each cumulative data point was corrected for the effect of dilution from previous collections of data points. Each release study experiment was run in triplicate.

2.9. *In Vitro* Biocompatibility

NIH3T3 cells were grown in DMEM containing 4.5 g/L glucose and GlutaMAX™ (Gibco) supplemented with 2% (v/v) PennStrepp (Sigma-Aldrich) and 10% (v/v) fetal bovine serum (Gibco). Cells were cultured at 37 °C, in a 5% CO_2 incubator, trypsinized at about 90% confluency, and split at 1:5 or 1:6 ratio.

Complete DMEM medium containing DCC, CDAC, or a mixture of DCC and CDAC was prepared by dilution of autoclaved stock dispersions. The highest concentration of DCC and CDAC in complete DMEM was 0.9 mg/mL, which was further serially diluted to a concentration of 28.125 µg/mL. Dispersions containing mixture of DCC and CDAC were prepared by mixing equal volume of DCC and CDAC dispersions at the same concentration. All dispersions were vortexed to homogenize and stored in the fridge for 24 h.

Cells were seeded in a 96-well plate at a density of 8000 cells/well. After 24 h, medium was removed and cells were washed once with 200 µL of PBS. Afterwards, 200 µL of nanocellulose-containing DMEM was added to each well. Cells were then left to proliferate for 48 h.

After 48 h, the nanocellulose-containing medium was removed. Cells were washed once with PBS, added with 100 µm of complete DMEM containing 10% v/v AlamarBlue and incubated for 4 h. The fluorescence intensity of resorufin (i.e. metabolically reduced resazurin) was then recorded using a Victor^3 plate reader (PerkinElmer, USA). Cells grown in complete DMEM without nanocellulose were regarded as positive controls. All recorded fluorescence intensities were corrected by subtracting the values with those of no-cell control wells. All cell experiments were carried out in triplicates.

To study the morphology of 3T3 cells following 48 h of treatment with various CNFs at the highest concentration of 900 µg/mL, the cells were washed, stained with Hoechst 33342 and propidium iodide, and imaged under a cellSense fluorescence microscope (Olympus, Japan). Images were further processed using ImageJ/FIJI (National Institute of Health, MD) [15].

2.10. Statistical Analysis

Data were analyzed and plotted with the GraphPad Prism version 6.01 software. All data represent means ± standard deviation. Statistical significance analysis was performed based on the two-sample *t*-test and the difference was considered to be significant when $p < 0.05$.

3. Results and Discussion

3.1. Syntheses of DCC and CDAC

All six CNF derivatives were stable in their dispersions in deionized water at typical concentration of ~0.7% w/w, kept at 4 °C, and used as such. Table 1 presents the final concentration, physical appearance, and content of the introduced functional group of each of the synthesized CNF. Based on the carboxylic acid content, up to 22% of anhydrous glucose units (AGU) in the cellulose (in case of DCC180) reacted. For CDAC, up to 29% (for CDAC180) of AGUs were functionalized with the cationic group.

Table 1. Physical and chemical properties of DCC and CDAC CNF dispersions, synthesized at different periodate oxidation durations.

Materials	Concentration after fibrillation	Appearance after fibrillation	[-COOH] or [-$N^+(CH_3)_3$] (mmol/g of dry sample)
DCC30	0.79% w/w	Gel-like viscous liquid	0.44
DCC120	0.74% w/w	Gel-like viscous liquid	0.89
DCC180	0.70% w/w	Gel-like viscous liquid	1.16
CDAC30	0.75% w/w	Milky white dispersion	0.26
CDAC120	0.83% w/w	Milky white dispersion	0.70

CDAC180	0.74% w/w	More transparent dispersion	0.86

3.2. Nanofibril Morphologies Based on Atomic Force Microscopy

CNF dispersions often contain a mixture of fractions of different sizes/morphologies, which is partly due to incomplete fibrillation [17, 18]. Collectively, these fractions influence the final properties of the CNF dispersions. AFM images of the six CNFs showed distinct fractions of nanofibrils (Figure 1). Some nanofibrils were isolated, with two distinguishable ends for practical measurement of length, while another fraction contained highly entangled/aggregated nanofibrils. Further, partial or incomplete fibrillation was also observed in several instances as shown, for example, in Figure 1d.

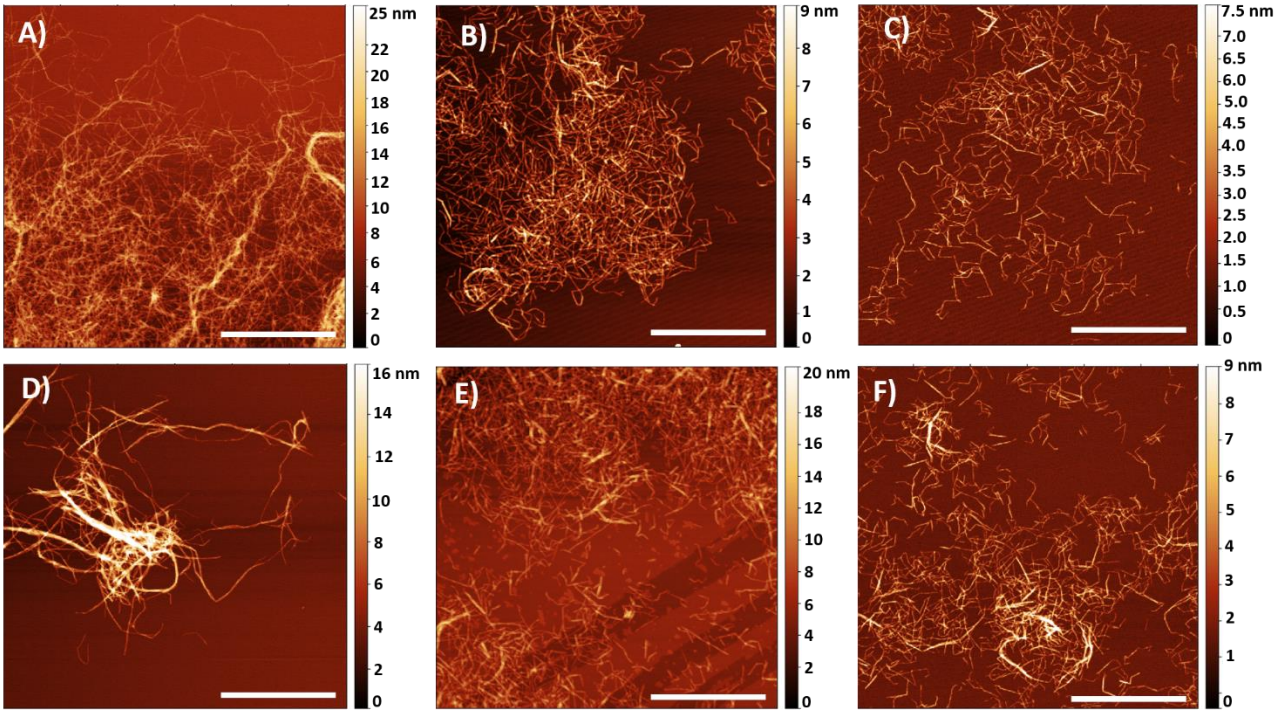

Figure 1. AFM images of (A) DCC30, (B) DCC120, (C) DCC180, (D) CDAC30, (E) CDAC120, and (F) CDAC180, which show two fractions of nanofibrils: highly entangled nanofibrils and isolated shorter nanofibrils. (D) shows a typical example of CNF with incomplete fibrillation. Scale bars = 2 µm.

For length estimation, entangled nanofibrils were not included in the measurement, as it is impossible to determine two possible ends of an individual nanofibril. However, the presence of this fraction of entangled nanofibrils is important, as they constitute a large part of the system and contribute to the observed gel-like network integrity in their aqueous dispersions. On the other hand, width measurements include also the entangled nanofibrils. We found that, apart from the occasional high values obtained from partially fibrillated fraction, the widths of nanofibrils were relatively consistent, as will be discussed in more detail below. Histograms of populated widths and lengths of each CNF are presented in Figure 2.

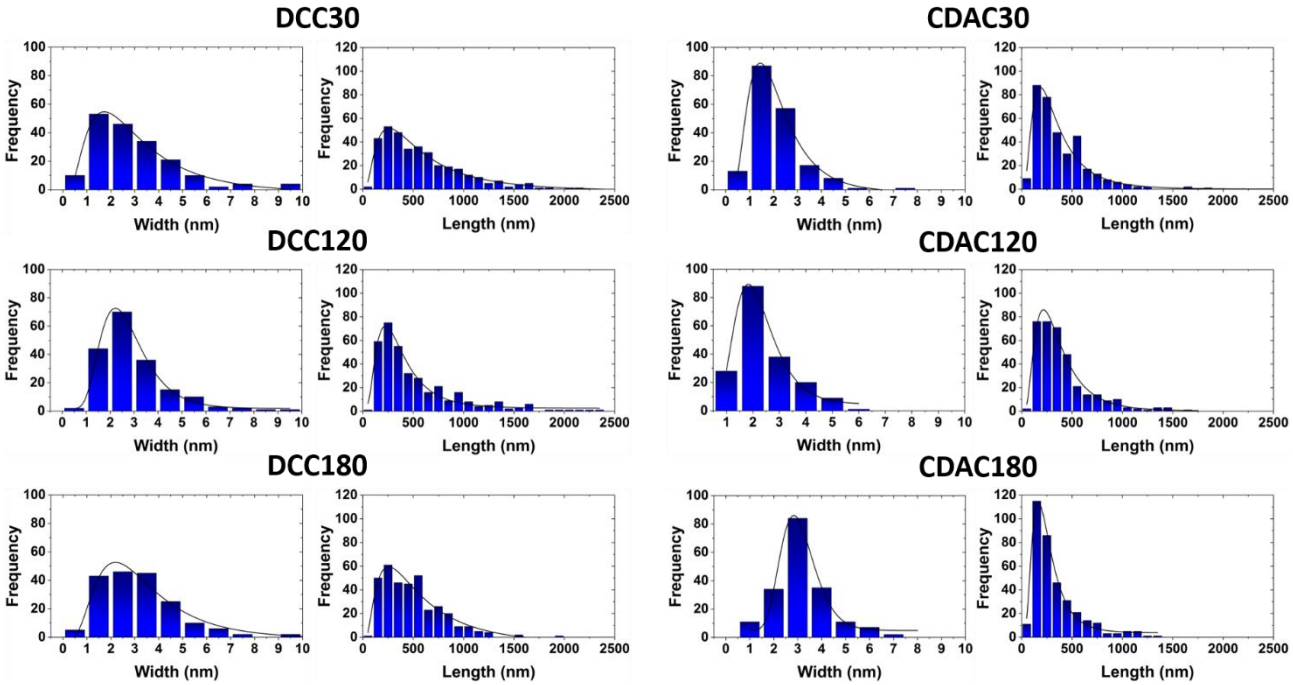

Figure 2. Width and length distribution histograms of DCC30, DCC120, DCC180, CDAC30, CDAC120, and CDAC180. The continuous curve in each histogram represents the curve fitting result with lognormal function.

We employed three different methods for estimating the widths and lengths of the CNFs. The first method involves fitting the histogram using the lognormal distribution function as a probability distribution often used for describing particle size distributions [19-21]. As can be observed from the continuous curves shown in Figure 2, all length and width distributions appropriately fit the lognormal function. From each fitted curve, a peak center value was then retrieved as listed in Table 2. The second and third methods were by calculating the number average and length-weighted average length and width from the populated AFM data. The polydispersity index (PDI) was then calculated as the ratio of length-weighted average to the number average. Table 2 displays the widths and lengths of the CNFs, as well as the calculated PDI.

Table 2. Width and length of DCC30, DCC120, DCC180, CDAC30, CDAC120, and CDAC180, obtained from fitting with lognormal function, calculation of number average, length-weighted average, and the corresponding PDI. μ represents the population mean, and σ represents the population standard deviation.

CNF		Lognormal fit	Number average		Length-weighted average (nm)	PDI
		Peak center (nm)	μ (nm)	σ/μ (%)		
Width	DCC30	2.8	2.12	48	2.61	1.23
	DCC120	2.6	2.42	42	2.87	1.19
	DCC180	3.1	3.18	36	3.63	1.14
	CDAC30	1.9	3.01	58	4.05	1.35
	CDAC120	2.1	2.95	49	3.66	1.24
	CDAC180	3.0	3.19	53	3.96	1.24
Length	DCC30	521.2	591	70	807	1.37
	DCC120	329.6	527	78	844	1.60
	DCC180	520.8	490	58	656	1.34
	CDAC30	300.8	390	77	623	1.60
	CDAC120	320.3	401	67	579	1.44
	CDAC180	229.6	334	72	371	1.11

As shown in Table 2, there is no clear relationship between the duration of oxidation and the width of resulting nanofibrils. The three different methods that were employed also showed relatively comparable

values. For all CNFs, nanofibril lengths were between 2-4 nm. This indicates that the observed nanofibrils are mostly elementary nanofibrils [22] and that the chemical pretreatments incorporated are highly efficient to help delaminate cellulose pulps, even at a low duration of oxidation.

Regarding length estimation, despite the proper fit of the lognormal distribution function, the peak center values did not show any apparent trend in the effect of oxidation duration. On the other hand, number and length-weighted average values displayed relatively apparent trend of decreasing length with longer oxidation duration. These results indicate that longer periodate oxidation duration leads to shorter nanofibrils. As the width of nanofibrils did not considerably change and had already reached elementary nanofibril width with the lowest oxidation duration, longer periodate oxidation duration likely led to more extensive dissolution of intrafibrillar amorphous regions. Further extent of reaction, which can be achieved, for example, by increasing the reaction temperature, can be expected to result in cellulose nanocrystals (CNC).

The PDI values (Table 2) indicate a general trend of decreasing PDI with increasing periodate oxidation duration. This may indicate that both width and length became more monodisperse with longer periodate oxidation. However, it is also worth noting that the change in width polydispersity is less prominent than the change in length polydispersity. This result aligns with the previous discussion regarding how width remains relatively constant, but length decreases as periodate oxidation duration increases.

Typically, we found that CDAC nanofibrils had an average length of ~300-600 nm, while DCC nanofibrils had an average length of ~500-800 nm. This may indicate that Girard's reagent T, which has a permanent charge, is more efficient in facilitating pulp delamination. Additionally, CDAC was nanofibrillated through a 100-µm interaction chamber instead of the 200-µm used on DCC, which possibly led to more extensive fibrillation. The observed trend of decreasing nanofibril length with increasing functional group content and chemical pretreatment duration aligns with the results of pervious studies on both CNF and CNC [18, 21, 23-25].

3.3. Hydrogel Formation and Rheological Properties

We investigated the viscoelastic properties of hydrogels prepared in different buffers using a rheometer. To conduct a comparison, the viscoelastic properties of the individual DCC and CDAC dispersions before mixing were also recorded. Frequency sweep (Figure 3a, right) was carried out within the linear viscoelastic region (Figure 3a, left) of each gel or CNF dispersion (γ = 1%) to obtain the storage modulus (G') and loss modulus (G"). The values of G' and G" at the angular frequency of 9.96 rad/s were used for comparisons among systems, as shown in Figure 3b and c.

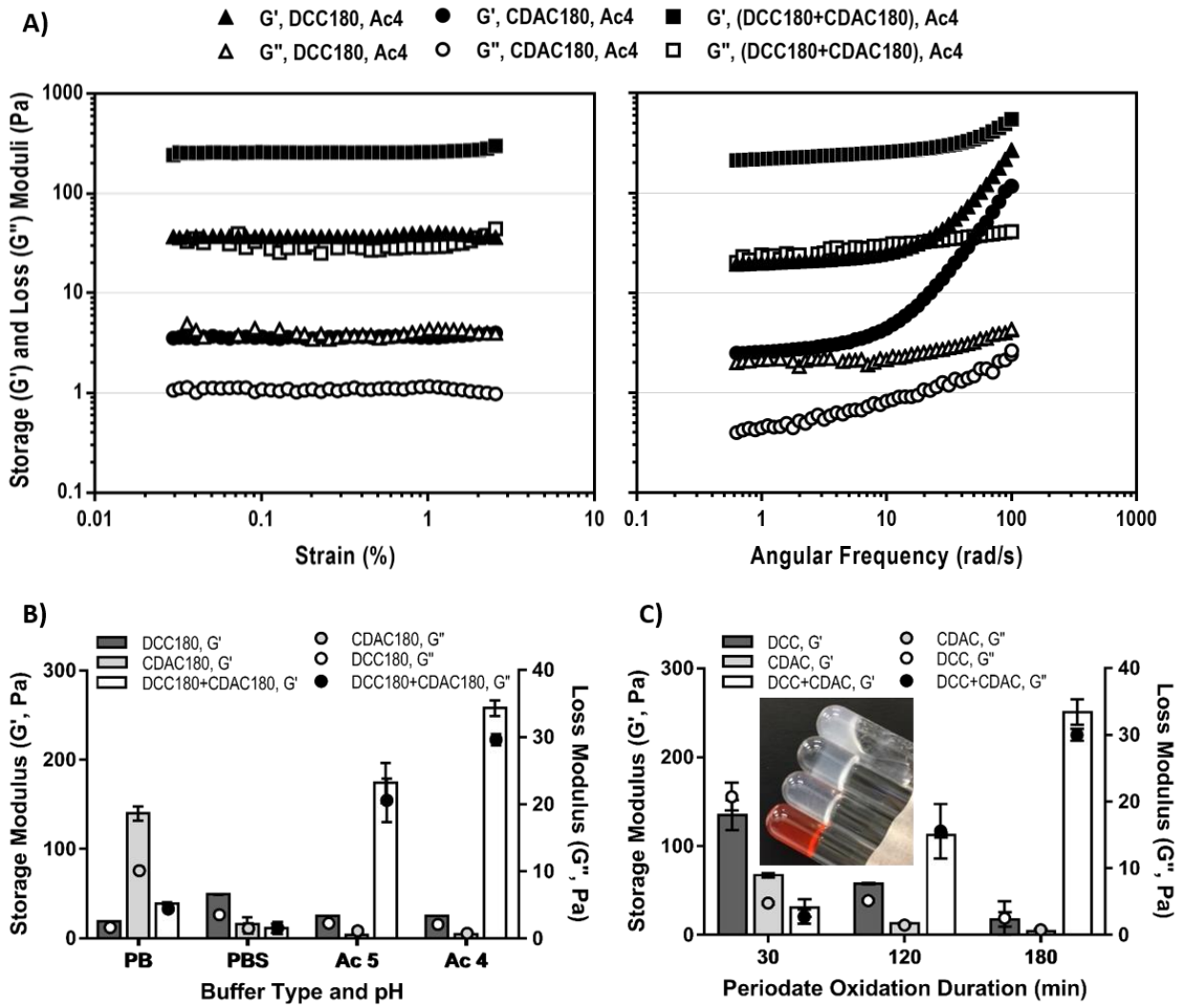

Figure 3. (A) Typical strain sweep (left) and frequency sweep (right) profiles of individual DCC180 and CDAC180 dispersions, and the (DCC180+CDAC180) gel. (B) G' and G" values of (DCC180+CDAC180) hydrogels, and the individual DCC180 or CDAC180 dispersions at various pH values and ionic strength conditions. (C) G' and G" values of (DCC+CDAC) hydrogels prepared in acetate buffer pH 4 using DCC and CDAC prepared at different oxidation durations. Some error bars are smaller than their symbols. Inset shows the visual appearance of tilted hydrogels; from top to bottom: (DCC30+CDAC30) gel, (DCC120+CDAC120) gel, (DCC180+CDAC180) gel, DOX-loaded (DCC180+CDAC180) gel.

3.3.1. Effect of pH, salt, and oxidation duration on monocomponent CNF dispersions

We noted that, while individual DCC cellulose nanofibrils were typically viscous and gel-like, they did not form self-standing gels and would flow if given enough time, especially at the low concentration of 0.5% w/w. This property of individual CNF is demonstrated through oscillatory rheology, as depicted in Figure 3b and c. The storage moduli of individual CNF in various buffer types were relatively low, below 50 Pa, except for CDAC180 in PB (Figure 3b) and DCC30 in Ac4 (Figure 3c), which showed higher G'. This result agrees with those of various reports on similar CNFs [26-28] and is relatively constant throughout the pH range that was studied (pH 7.4, 5, and 4) (Figure 3b). It is likely that in this pH range, electrostatic repulsion from ionic groups inhibits physical crosslinking. For DCC, because the pKa of carboxylic acid is around 3.5 [29], more extensive physical crosslinking (i.e. nanofibril aggregation due to reduced surface charge or more extensive hydrogen bonding) can be expected below this pH, as reported by Wågberg and coworkers [30]. On the other hand, for CDAC, the permanent charge provided by the quaternary ammonium ion can inhibit gelation in aqueous condition.

The presence of salt in DCC180 dispersion at pH 7.4, as demonstrated in the use of PBS buffer, also did not significantly improve gelation (Figure 3b). It has been suggested that salt can help mask the charge repulsion in carboxylic acid-containing CNF, and thus facilitate gelation [30]. We did observe a slight increase in G' of DCC180 in PBS as compared to that of DCC180 in PB (Figure 3a). However, it is likely that in our case, the concentration of carboxylic acid group was too high and thus more salt was needed to significantly increase the gelation properties of DCC180 at pH 7.4. We did not increase the salt concentration to adhere more closely to the relevant physiological conditions.

We further investigated the gelation properties of other individual DCCs and CDACs at pH 4. As can be observed in Figure 3c, longer periodate oxidation duration led to decreasing moduli of individual CNF dispersions. As the oxidation duration increases, the degree of functionalization increases (Table 1) and, consequently, more charge-repulsion takes place, resulting in weaker nanofibril network integrity. Furthermore, increasing oxidation duration also resulted in relatively shorter nanofibril lengths (Table 2). Shorter nanofibrils lengths have been reported to lead to lower intrinsic viscosity of CNF dispersions [31]. Shorter nanofibrils entangle less and thus the resulting network is weaker and less able to maintain network integrity, thereby lowering the intrinsic viscosity. This is also reflected in the decrease in moduli for the individual DCC and CDAC dispersions as periodate oxidation duration increased (Figure 3c). In this specific case of study, we believe that CNF length and charge density are the two main factors that contribute in the gelation properties of these monocomponent CNF dispersions. Other factors possibly also play a role, which need more detail investigation, but this falls outside the scope of this study.

3.3.2. Effect of pH, salt, and oxidation duration on polyion complex hydrogels

Mixing DCC180 and CDAC180 at pH 7.4, both in the presence and absence of salt, did not result in self-standing gels. We predicted that at this pH, the quaternary ammonium ion may ionically crosslink deprotonated carboxylic acid, which would result in more pronounced gelation. However, it is likely that the nanofibrils are stiffer than a typical polyelectrolyte that an ideal arrangement of ionic crosslinks is more difficult to achieve.

Interestingly, by lowering the pH to 5 and 4, a noticeable increase in gelation is observed for the bicomponent gels (Figure 3b). Since each individual CNF dispersion did not form self-standing gels, formation of gels on bicomponent system can only be attributed to possible ionic crosslinking between quaternary ammonium ion of CDAC and deprotonated carboxylic acid of DCC. We also note that stronger gels were formed at pH 4 than at pH 5, which indicates that nanofibril aggregation (physical crosslinking through hydrogen bonding) [30], in relation to reduced charge-repulsion in DCC at a lower pH, may play an important synergistic role with ionic crosslinking in maintaining a more robust 3D network of CNF. It can be predicted that higher portion of protonated carboxylic acid of DCC leads to more hydrogen bonds not only between DCCs, but also between DCC and CDAC. This masks the effect of charge-charge repulsion between quaternary ammonium groups, while at the same time allowing nearby carboxylic acid groups to exert more ionic character to facilitate ionic crosslinking.

In terms of the effect of oxidation duration on gelation at pH 4, individual CNF dispersions were weaker and more liquid-like as oxidation duration increased. In contrast, we observed the opposite trend for the polyion complex gels. Stronger gels were obtained by mixing DCC and CDAC that went through longer oxidation duration. It is very likely that the effect of charge repulsion in the CNF dispersions before mixing was counteracted by the presence of ionic crosslinks in the bicomponent gels. As the content of ionic or ionizable group increases with increasing periodate oxidation duration (Table 1), the extent of ionic crosslinking also increases, thus resulting in stronger gels (Figure 3c).

Figure 3c (inset) shows the physical appearances of various (DCC+CDAC) gels prepared at pH 4 in the fashion of a vial-tilting test. It can be observed that gels prepared from DCC30 and CDAC30 could not

maintain network integrity and behaved more like a liquid rather than a solid. (DCC120+CDAC120)Ac4 gels were solid-like but had two separate phases: a more transparent DCC-rich lower phase, and a more turbid CDAC-rich upper phase. The appearance of the two phases indicates non-homogeneous mixing, which is likely due to the large difference in viscosities of the two components. In contrast, (DCC180+CDAC180)Ac4 gels were homogeneous. When (DCC180+CDAC180)Ac4 gels were loaded with orange-colored DOX, the incorporated DOX was homogeneously distributed throughout the gel.

To obtain a closer look into the CNF-based gels, we subjected (DCC180+CDAC180)Ac4 gels, with and without DOX, to FESEM imaging. The images, shown in Figure 4, showed two types of structures, i.e. sheet-like structures and fibrillar structures. The FESEM samples were obtained after freeze-drying the gels and are therefore not a correct representation of the gels in the hydrated state. However, we can observe that the surface of sheet-like structures from DOX-loaded gels (Figure 4b.1) appeared rougher than that from gels without DOX (Figure 4a.1), indicating the presence of DOX that was homogeneously distributed on the sheets, and most likely, throughout the network in its hydrated state. The sheet-like structure is a characteristic of freeze-dried CNF aerogels [32]. We propose that the sheet-like morphologies (Figure 4a.1 and Figure 4b.1) were induced by the freeze-drying process and thus the nanofibril structures (Figure 4a.2 and Figure 4b.2) are a closer depiction of the native hydrated state of the gels. The nanofibrils are highly entangled but leave empty spaces as pores that can retain medium. These nanofibril structures are relatively similar to the obtained AFM images of nanofibril bundles (Figure 1), confirming the prominent existence of fractions of aggregated nanofibrils. Further, nanofibrils are long and can be observed to be in the micrometer-range.

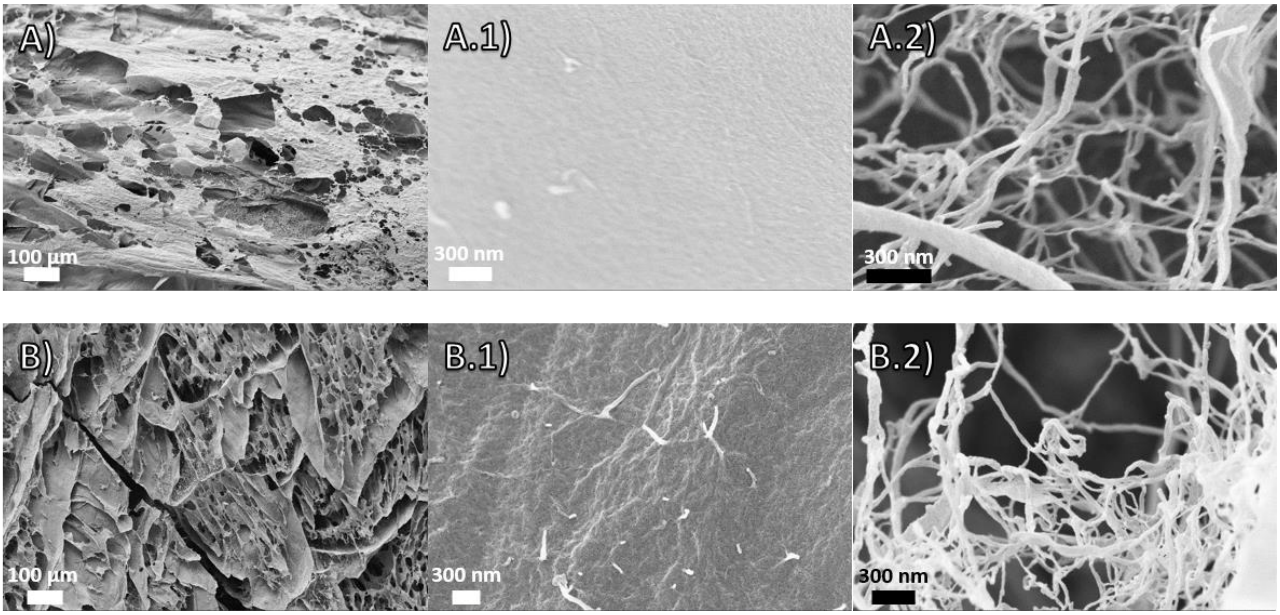

Figure 4. FESEM images of (DCC180+CDAC180)Ac4 gels, with (A) and without (B) DOX. (1) Higher magnification of sheet surface, and (2) Higher magnification of nanofibril structures.

3.4. Doxorubicin Release Profiles

To demonstrate the ability of the prepared gels to provide controlled or sustained release of therapeutic agents, DOX, which is a small, amine-containing chemotherapeutic agent, was loaded into (DCC180+CDAC180)Ac4 gels by first dissolving DOX into DCC180 dispersion in Ac4 before mixing with CDAC180. Upon mixing, gelation took place thereby entrapping the DOX within the self-standing hydrogel matrix. This way, loading efficiency into the hydrogels is always 100%, and the amount of loaded therapeutic agent can be easily adjusted according to patient-specific prescriptions.

For this study, the concentration of DOX in the DCC180 dispersion was 800 µg/mL, making the final DOX content in a 1 mL (DCC180+CDAC180)Ac4 gel to be 400 µg/1 mL gel. DOX-loaded gels were scooped out of the tube and immersed into 10 mL of buffer solution as shown in Figure 5. Two types of media were chosen to investigate pH-responsive release: PBS buffer pH 7.4 and acetate buffer saline (ABS) pH 4. Both media contained 150 mM of salt to mimic physiological salt concentration.

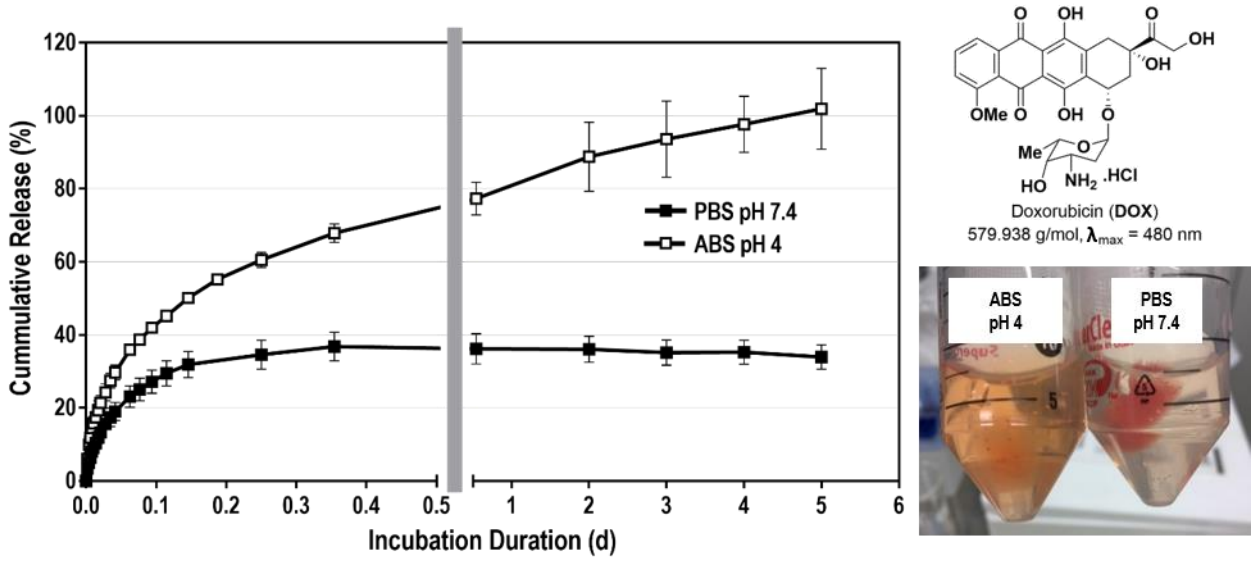

Figure 5. Release profiles of DOX in PBS pH 7.4 and ABS pH 4, chemical structure of DOX, and a photograph of gels in the respective release media 1 day (ABS pH 4) and 2 days (PBS pH 7.4) since the start of incubation. Lines in the release curves are provided to guide the eyes.

As shown in the plots of release profiles in Figure 5, DOX-loaded (DCC180+CDAC180)Ac4 gels released DOX at different rates depending on the pH of the release media. In PBS pH 7.4, burst phase was observed for the first 6 h, during which roughly 35% of the DOX content was released and after which no further release was detected. Meanwhile, in ABS pH 4, an initial fast release in combination with a burst phase were observed for the first 8.5 h but were later followed by a slower, more sustained release until a complete release was achieved on day 5.

Due to the absence of chemical crosslinks, it can be predicted that (DCC+CDAC) hydrogels may be prone to swelling and dissolution in aqueous media. However, we found that (DCC180+CDAC180)Ac4 gels did not swell considerably, and erosion took place mainly with help from mechanical interference (data not shown). We propose that, compared to water-soluble macromolecular chains of polyelectrolytes, CNFs have inherently less mobility in aqueous medium due to their relatively larger dimensions. When further supported by ionic crosslinks, nanofibril entanglement and aggregation, this leads to a more robust 3D integrity.

Without considerable swelling of the hydrogel matrix, upon complete release of DOX into the pH 4 medium, the empty 'shell' of the gel remained suspended in the medium. We can therefore predict that the release mechanism of DOX from these gels is mostly diffusion-based. Indeed, when we fit the cumulative release profile ($^{M_t}/_{M_\infty}$ < 0.6) in ABS pH 4 into the Peppas equation:

$$\frac{M_t}{M_\infty} = kt^n \qquad (1)$$

$$\ln\left(\frac{M_t}{M_\infty}\right) = k' + n\ln(t) \qquad (2)$$

where M_t/M_∞ is the fraction of drug released at time *t*, we found *n* to be 0.476 at R^2 of 0.989, which is close to the theoretical value of *n* for Fickian diffusion from a cylinder [33, 34].

The faster release of DOX in acidic pH as opposed to pH 7.4 has been previously reported [35-37]. DOX has an amine group with reported pK_a of ~8.3 [38, 39] and thus is mostly protonated at both pH 7.4 and pH 4. At pH 7.4, DOX release is hindered due to the interaction between DOX and deprotonated carboxylic acid group within the gel. In contrast to the quaternary ammonium ion in CDAC, which is stiffer and immobilized on the surface of the nanofibrils, the small and fully dissolved DOX can more efficiently diffuse for optimal interaction with deprotonated carboxylic acid on DCC, minimizing potential repulsion with the positively charged quaternary ammonium ion. Thus, at pH 7.4, only DOX molecules that are loosely bound and located on the outer surface of the gels are released, which accounts for 35% of the total loaded DOX. At pH 4, a higher portion of carboxylic acid in the gel is protonated and thus there is less interaction with the DOX, which enables DOX to diffuse out of the porous matrix. Higher solubility of DOX in acidic medium, due to a higher degree of amine protonation, likely also enhances its diffusion from the hydrogel matrix.

The enhanced release profile of DOX from the (DCC180+CDAC180)Ac4 gels at acidic pH can be exploited to provide more pronounced release in acidic pathophysiological conditions, such as in tumor tissue, which is known to be slightly more acidic than normal healthy tissue [40]. The (DCC+CDAC) matrix in this case serves to inhibit release in healthy tissue to prevent adverse effects of the cytotoxic agent. We also believe that the versatility of (DCC180+CDAC180)Ac4 matrix in providing controlled release can be extended to other therapeutic agents.

3.5. Biocompatibility of CNF Hydrogels

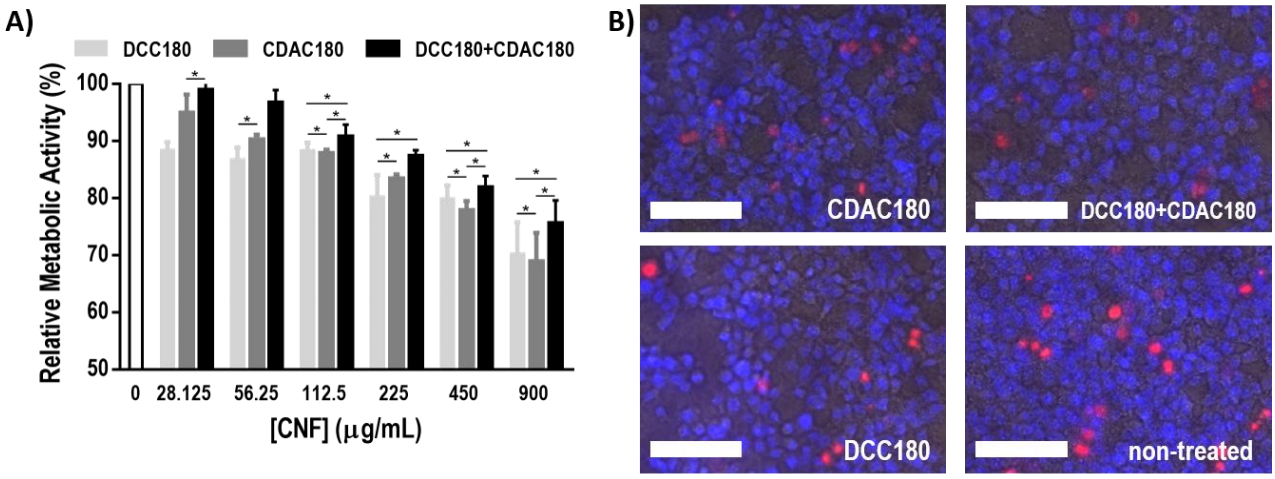

*Figure 6. (A) Metabolic activity of NIH3T3 cells after 48 h of treatment with CNF at various concentrations, relative to the metabolic activity of non-treated (Ctrl) cells. *Not significantly different from one another ($p > 0.05$), (B) Fluorescence microscopy images of NIH3T3 cells at the end of 48 h of treatment with or without CNFs. CNF treatment was conducted at a concentration of 900 μg/mL. Live cells were stained for their nuclei with Hoechst 33342 (blue), and dead cells were stained with propidium iodide (red). Scale bars = 100 μm.*

To evaluate the suitability of DCC180 and CDAC180 as biomaterials for drug delivery applications, an assessment of their biocompatibility was conducted. *In vitro* biocompatibility of DCC180, CDAC180, and their combination were investigated by suspending nanocellulose directly into the cell culture media that were then introduced into a culture of NIH3T3 cells. Nanocellulose concentrations were varied from a maximum of 900 μg/mL through serial dilution. The metabolic activity of cells that have been incubated with CNF-containing media for 48 h was quantified using the AlamarBlue assay. In this assay, resazurin is metabolically reduced by live cells into resorufin ($\lambda_{ex}/\lambda_{em}$ = 545/590 nm), and the fluorescence intensity of resorufin is an indication of the overall metabolic activity of the cell population. The relative metabolic

activity of cells treated with CNF at a certain concentration is then calculated as the percentage of resorufin fluorescence intensity relative to non-treated cells. In Figure 6a, non-treated cells are shown as cells which had been treated with 0 μg/mL CNF and the recorded fluorescence intensity was regarded as 100%.

As can be seen from Figure 6a, all the nanocellulose samples at the tested concentrations induced viability of at least 70%, relative to cells grown without any of the gel materials, which indicates non-cytotoxicity according to the International Organization for Standardization (ISO) standard [41]. Figure 6b further compares the cell morphology at the end of the 48-h treatment with or without CNF. No significant differences in morphology can be observed, but there is a clear difference in the number of live cells among the samples. The negative control well, in which cells were not treated with CNF, showed a confluent cell monolayer, in contrast to CNF-treated wells, in which less live cells were visible. Due to the tendency of the nanocellulose to aggregate and form viscous gel-like dispersion, the decrease in metabolic activity could be caused by hindered gas exchange that occurs as nanocellulose forms additional barrier across the medium. Similar results have been reported for nanocellulose-containing hydrogels where similar range of concentration of material was studied, but metabolic activity was measured after only one day of exposure, instead of two [42].

The reported result adds to a growing literature that indicates a general biocompatibility profile of nanocellulose-based materials. We note that the two oppositely charged CNFs and their mixture did not show any significant difference in cytocompatibility profiles (Figure 6a). We hypothesize that the high tendency of CNF to attract water and maintain a 3D network leads to a significant masking of the surface charges of the nanofibrils. As a result, cells may not come in direct contact with the nanofibrils as readily and are thus less affected by the surface functionalization on the nanofibrils. This result suggests the prospect of exploring potential chemical derivatives of cellulose nanofibrils for various biomedical applications.

The cytotoxicity of DOX-loaded gels was not studied in this current report. The current study was aimed predominantly at studying the CNFs as potential components for fabrication of self-standing hydrogels and their optimizations for biomedical applications. The DOX used in this study was meant as a model to demonstrate the feasibility of utilizing CNF-based self-standing hydrogels as a matrix for controlled drug release. DOX was also a practical choice as it is a colored compound, making detection and accurate calculation of concentration quite straightforward through UV-Vis spectrophotometry. Additionally, doxorubicin is relatively stable and can be assumed to maintain its therapeutic efficacy during the experiments. With a better understanding on the system, we believe the most appropriate application for the system can be envisioned. We hope that the current report can provide a start from which more clinically relevant investigations on the system can be designed and accomplished.

4. Conclusion

We have presented a new type of polyion complex hydrogels from two complementary derivatives of cellulose nanofibrils and demonstrated their ability to provide sustained and pH-responsive release of doxorubicin, which is an anticancer drug. Two types of cellulose nanofibrils were synthesized: carboxylic acid-containing DCC and quaternary ammonium-containing CDAC. The extent of chemical modification was successfully varied by choosing different periodate oxidation durations, which also led to different morphologies, particularly length. AFM characterizations showed that the majority of CNFs were elementary nanofibrils with a width of approximately ~2-4 nm. Two distinct fractions were present in each CNF dispersion: nanofibril bundles and shorter less-entangled nanofibrils. The latter fraction was used for length estimation, leading to an average length of ~500-800 nm for DCC and ~300-600 nm for CDAC.

Monocomponent dispersions of cellulose nanofibrils showed decreasing loss and storage moduli as the periodate oxidation duration increased, demonstrating the role of charge-charge repulsion and physical entanglement in the viscoelastic properties of the cellulose nanofibrils in aqueous dispersions. However, when DCC and CDAC were mixed, the opposite trend occurred, where increasing periodate oxidation duration led to higher loss and storage moduli. This indicates the more pronounced role of ionic crosslinking compared to simple physical entanglement. The strongest mixed DCC and CDAC gels were obtained at pH 4, indicating that nanofibril aggregation and hydrogen bonding, which is more enhanced at acidic pH when more of the carboxylic acids are protonated, also played an important role.

Doxorubicin entrapped during hydrogel formation displayed a pH-dependent release profile. At pH 7.4, only 35% of incorporated DOX was released in a burst phase for the first 6 h, and further release was not detected. At pH 4, DOX release was faster for the first 8.5 h, and then slower for up to 5 days when all of the DOX was released. At pH 4, DOX was released by diffusion. At both pH 4 and 7.4, no significant swelling or surface erosion was detected. 3D integrity was likely maintained by the synergistic effect of nanofibril aggregation and entanglement, as well as ionic crosslinks between the complementary CNFs.

We further showed that DCC180 and CDAC180, either individually or in combination, at concentrations as high as 900 µg/mL, were nontoxic to NIH3T3 cells *in vitro*. Our results confirm the potential applicability of nanocellulosic materials as green, naturally derived biomaterials for biomedical applications.

As a drug delivery system, we have shown that the CNF-based polyion complex hydrogels are able to serve as a self-standing matrix for controlled drug release at a relatively low concentration of 0.5% w/w. When used to incorporate DOX, the gels also provide pH-responsive release profiles, with more pronounced release at acidic pH. However, we note that the polyion complex hydrogels are not self-healing, owing to the robust ionic crosslinks facilitated by dispersed CNFs, and are therefore not readily injectable. As such, these gels could be implanted within a tumor tissue as a pH-responsive depot for release of DOX. Alternatively, the use of double-barrel syringes could be envisioned for a more minimally invasive administration *via* injection.

5. Author Information

Corresponding Author

*E-mail: Henrikki.Liimatainen@oulu.fi

Notes

The authors declare no competing financial interest.

6. Acknowledgement

The authors would like to thank Dr. Juho Antti Sirviö for help with syntheses of the CNFs, Mrs. Elisa Wirkkala for performing elemental analysis, Ms. Tuula Selkälä for help with AFM sample preparation, and Biocenter Finland for providing fluorescence microscopy facility used in this study. The authors kindly acknowledge financial support from the Academy of Finland (projects NanoBioMass (307535), CNT4Tissue, 206038, 121647, 250900 and 260056), the Sigrid Jusélius Foundation, and the European Community's Seventh Framework Program FP7/2009 under grant agreement 305608 (EURenOmics: European Consortium for High-Throughput Research in Rare Kidney Diseases).

7. References

[1] E. Caló, V.V. Khutoryanskiy, Biomedical applications of hydrogels: A review of patents and commercial products, European Polymer Journal 65(Supplement C) (2015) 252-267.

[2] R.J. Moon, A. Martini, J. Nairn, J. Simonsen, J. Youngblood, Cellulose nanomaterials review: structure, properties and nanocomposites, Chemical Society Reviews 40(7) (2011) 3941-3994.
[3] H. Wu, S. Liu, L. Xiao, X. Dong, Q. Lu, D.L. Kaplan, Injectable and pH-Responsive Silk Nanofiber Hydrogels for Sustained Anticancer Drug Delivery, ACS Applied Materials and Interfaces 8(27) (2016) 17118--17126.
[4] H. Paukkonen, M. Kunnari, P. Laurén, T. Hakkarainen, V.-V. Auvinen, T. Oksanen, R. Koivuniemi, M. Yliperttula, T. Laaksonen, Nanofibrillar cellulose hydrogels and reconstructed hydrogels as matrices for controlled drug release, International Journal of Pharmaceutics 532(1) (2017) 269-280.
[5] A.C. Borges, C. Eyholzer, F. Duc, P.-E. Bourban, P. Tingaut, T. Zimmermann, D.P. Pioletti, J.-A.E. Månson, Nanofibrillated cellulose composite hydrogel for the replacement of the nucleus pulposus, Acta Biomaterialia 7(9) (2011) 3412-3421.
[6] H. Mertaniemi, C. Escobedo-Lucea, A. Sanz-Garcia, C. Ganda, A. Mkitie, J. Partanen, O. Ikkala, M. Yliperttula, Human stem cell decorated nanocellulose threads for biomedical applications, Biomaterials 82 (2016) 208--220.
[7] M. Bhattacharya, M.M. Malinen, P. Lauren, Y.R. Lou, S.W. Kuisma, L. Kanninen, M. Lille, A. Corlu, C. GuGuen-Guillouzo, O. Ikkala, A. Laukkanen, A. Urtti, M. Yliperttula, Nanofibrillar cellulose hydrogel promotes three-dimensional liver cell culture, J Control Release 164(3) (2012) 291-8.
[8] M. Kimura, Y. Shinohara, J. Takizawa, S. Ren, K. Sagisaka, Y. Lin, Y. Hattori, J.P. Hinestroza, Versatile Molding Process for Tough Cellulose Hydrogel Materials, Scientific Reports 5(1) (2015) 16266.
[9] R. Kolakovic, T. Laaksonen, L. Peltonen, A. Laukkanen, J. Hirvonen, Spray-dried nanofibrillar cellulose microparticles for sustained drug release, International Journal of Pharmaceutics 430(1) (2012) 47-55.
[10] N. Lin, A. Dufresne, Supramolecular Hydrogels from In Situ Host − Guest Inclusion between Chemically Modified Cellulose Nanocrystals and Cyclodextrin, Biomacromolecules 14 (2013) 871--880.
[11] J. Leppiniemi, P. Lahtinen, A. Paajanen, R. Mahlberg, S. Metsa-Kortelainen, T. Pinomaa, H. Pajari, I. Vikholm-Lundin, P. Pursula, V.P. Hytonen, 3D-Printable Bioactivated Nanocellulose-Alginate Hydrogels., ACS applied materials \& interfaces (2017).
[12] O. Aarstad, E. Heggset, I. Pedersen, S. Bjørnøy, K. Syverud, B. Strand, Mechanical Properties of Composite Hydrogels of Alginate and Cellulose Nanofibrils, Polymers 9(8) (2017) 378.
[13] A. Rattaz, S.P. Mishra, B. Chabot, C. Daneault, Cellulose nanofibres by sonocatalysed-TEMPO-oxidation, Cellulose 18(3) (2011) 585.
[14] S. Katz, R.P. Beatson, A.M. Scallon, The determination of strong and weak acidic groups in sulfite pulps, Svensk papperstidning 87(6) (1984) 48-53.
[15] J. Schindelin, I. Arganda-Carreras, E. Frise, V. Kaynig, M. Longair, T. Pietzsch, S. Preibisch, C. Rueden, S. Saalfeld, B. Schmid, J.-Y. Tinevez, D.J. White, V. Hartenstein, K. Eliceiri, P. Tomancak, A. Cardona, Fiji: an open-source platform for biological-image analysis, Nature methods 9 (2012) 676.
[16] T. Wagner, M. Hiner, xraynaud, thorstenwagner/ij-ridgedetection: Ridge Detection 1.4.0 (Version v1.4.0), Zenodo, 2017.
[17] F. Jiang, T. Kondo, Y.-L. Hsieh, Rice Straw Cellulose Nanofibrils *via* Aqueous Counter Collision and Differential Centrifugation and Their Self-Assembled Structures, ACS Sustainable Chemistry & Engineering 4(3) (2016) 1697-1706.
[18] H. Fukuzumi, T. Saito, A. Isogai, Influence of TEMPO-oxidized cellulose nanofibril length on film properties, Carbohydrate Polymers 93(1) (2013) 172-177.
[19] R. Bienert, F. Emmerling, A.F. Thünemann, The size distribution of 'gold standard' nanoparticles, Analytical and Bioanalytical Chemistry 395(6) (2009) 1651.
[20] C. Zender, Particle Size Distributions: Theory and Application to Aerosols, Clouds, and Soils, 2001.
[21] S. Elazzouzi-Hafraoui, Y. Nishiyama, J.-L. Putaux, L. Heux, F. Dubreuil, C. Rochas, The Shape and Size Distribution of Crystalline Nanoparticles Prepared by Acid Hydrolysis of Native Cellulose, Biomacromolecules 9(1) (2008) 57-65.
[22] D. Klemm, F. Kramer, S. Moritz, T. Lindström, M. Ankerfors, D. Gray, A. Dorris, Nanocelluloses: A New Family of Nature-Based Materials, Angewandte Chemie International Edition 50(24) (2011) 5438-5466.
[23] R. Shinoda, T. Saito, Y. Okita, A. Isogai, Relationship between Length and Degree of Polymerization of TEMPO-Oxidized Cellulose Nanofibrils, Biomacromolecules 13(3) (2012) 842-849.

[24] H. Liimatainen, M. Visanko, O.E.O. Hormi, J. Niinimaki, Enhancement of the Nano fibrillation of Wood Cellulose through Sequential Periodate − Chlorite Oxidation, Biomacromolecule (13) (2012) 1592--1597.
[25] K. Conley, M.A. Whitehead, T.G.M. van de Ven, Chemically peeling layers of cellulose nanocrystals by periodate and chlorite oxidation, Cellulose 23(3) (2016) 1553-1563.
[26] E. Lasseuguette, D. Roux, Y. Nishiyama, Rheological properties of microfibrillar suspension of TEMPO-oxidized pulp, Cellulose 15(3) (2008) 425-433.
[27] M.P. Lowys, J. Desbrières, M. Rinaudo, Rheological characterization of cellulosic microfibril suspensions. Role of polymeric additives, Food Hydrocolloids 15(1) (2001) 25-32.
[28] G. Agoda-Tandjawa, S. Durand, S. Berot, C. Blassel, C. Gaillard, C. Garnier, J.L. Doublier, Rheological characterization of microfibrillated cellulose suspensions after freezing, Carbohydrate Polymers 80(3) (2010) 677-686.
[29] M. Towers, A.M. Scallan, Predicting the ion-exchange of kraft pulps using donnan theory, 1996.
[30] A.B. Fall, S.B. Lindstrom, O. Sundman, L. Odberg, L. Wagberg, Colloidal stability of aqueous nanofibrillated cellulose dispersions, Langmuir 27(18) (2011) 11332-8.
[31] J. Colson, W. Bauer, M. Mayr, W. Fischer, W. Gindl-Altmutter, Morphology and rheology of cellulose nanofibrils derived from mixtures of pulp fibres and papermaking fines, Cellulose 23(4) (2016) 2439-2448.
[32] O. Laitinen, T. Suopajärvi, M. Sterberg, H. Liimatainen, Hydrophobic, Superabsorbing Aerogels from Choline Chloride-Based Deep Eutectic Solvent Pretreated and Silylated Cellulose Nanofibrils for Selective Oil Removal, ACS Applied Materials and Interfaces 9(29) (2017) 25029--25037.
[33] P.L. Ritger, N.A. Peppas, A simple equation for description of solute release II. Fickian and anomalous release from swellable devices, Journal of Controlled Release 5(1) (1987) 37-42.
[34] P. Costa, J.M. Sousa Lobo, Modeling and comparison of dissolution profiles, European Journal of Pharmaceutical Sciences 13(2) (2001) 123-133.
[35] X. Hu, W. Wei, X. Qi, H. Yu, L. Feng, J. Li, S. Wang, J. Zhang, W. Dong, Preparation and characterization of a novel pH-sensitive Salecan-g-poly(acrylic acid) hydrogel for controlled release of doxorubicin, Journal of Materials Chemistry B 3(13) (2015) 2685-2697.
[36] L. Gao, Q. Sun, Y. Wang, W. Zhu, X. Li, Q. Luo, X. Li, Z. Shen, Injectable poly(ethylene glycol) hydrogels for sustained doxorubicin release, Polymers for Advanced Technologies 28(1) (2017) 35-40.
[37] H. Wang, Y. Zhao, Y. Wu, Y.-l. Hu, K. Nan, G. Nie, H. Chen, Enhanced anti-tumor efficacy by co-delivery of doxorubicin and paclitaxel with amphiphilic methoxy PEG-PLGA copolymer nanoparticles, Biomaterials 32(32) (2011) 8281-8290.
[38] S. Sanli, B. Akmese, N. Sanli, S.A. Ozkan, A Novel RP-LC Method for Determination of pK a Values of Some Anticancer Agents and Their Assay, Chromatographia 76(21) (2013) 1467-1475.
[39] N. Raghunand, B.P. Mahoney, R.J. Gillies, Tumor acidity, ion trapping and chemotherapeutics: II. pH-dependent partition coefficients predict importance of ion trapping on pharmacokinetics of weakly basic chemotherapeutic agents, Biochemical Pharmacology 66(7) (2003) 1219-1229.
[40] L.E. Gerweck, K. Seetharaman, Cellular pH Gradient in Tumor versus Normal Tissue: Potential Exploitation for the Treatment of Cancer, Cancer Research 56(6) (1996) 1194-1198.
[41] ISO10993-5. 2009, Part 5: Tests for in vitro cytotoxicity, Biological evaluation of medical devices, Association for the Advancement of Medical Instrumentation, Arlington, 2009.
[42] X. Yang, E. Bakaic, T. Hoare, E.D. Cranston, Injectable polysaccharide hydrogels reinforced with cellulose nanocrystals: Morphology, rheology, degradation, and cytotoxicity, Biomacromolecules 14(12) (2013) 4447--4455.